VERIZONA PUBLISHER
Publishing Your Ideas

www.verizonaonlinepublishing.com
Special Issue

Material Science and Engineering with Advanced Research

Effect of Solid Particle Erosion on the Aqueous Corrosion Behaviour of a Ti6Al4V Sheet

E Bata[1], K Lentzaris[1], AG Lekatou[1], NM Barkoula[2], A Poulia[1], AK Sfikas[1] and AE Karantzalis[1*]

[1]Laboratory of Applied Metallurgy, Department of Materials Science & Engineering, University of Ioannina, 45110 Ioannina, Hellas

[2]Laboratory of Composite and Smart Materials, Department of Materials Engineering, University of Ioannina

***Corresponding author:** AE Karantzalis, Laboratory of Applied Metallurgy, Department of Materials Science & Engineering, University of Ioannina, 45110 Ioannina, Hellas, Greece; Tel: (+30) 2651009026; Fax: (+30) 2651009082; E mail: akarantz@cc.uoi.gr

Article Type: Research, **Submission Date**: 15 February 2017, **Accepted Date:** 10 March 2017, **Published Date:** 23 May 2017.

Citation: E Bata, K Lentzaris, AG Lekatou, NM Barkoula, A Poulia (2017) Effect of Solid Particle Erosion on the Aqueous Corrosion Behaviour of a Ti6Al4V Sheet. Mater. Sci. Eng. Adv. Res Special Issue: 26-33. doi: https://doi.org/10.24218/msear.2017.4S.

Abstract

The economic and effective operation of machinery and plant involved in fluids handling is increasingly dependent on the utilization of materials that combine high corrosion resistance and good wear resistance.

The present study was undertaken in order to investigate the effect of solid particle erosion on the surface characteristics, the microstructure and the aqueous corrosion behavior of a Ti6Al4V sheet metal alloy. The scope of the present effort is to examine the possible way the solid particle erosion affect, by altering the Ti6Al4V surface characteristics, the subsequent electrochemical corrosion response.

As for the solid particle erosion tests, three (3) different impact angles were selected, 30°, 60° and 90° degrees respectively. Angular alumina particles of 177 – 250 μm size was used as the eroding media, injected, under 1 and 2 bars pressure, on the sample surface located at 10 mm distance from the injection nozzle. The mass loss was weighted and the wear rates were calculated. Surface roughness of the eroded surfaces was assessed and the microstructural modifications were evaluated using optical microscopy and SEM-EDX.

Cyclic polarization measurements were conducted in an electrolyte simulating body fluids in order to ascertain the corrosion response of the surface treated samples. SEM-EDX analysis of the corroded surfaces was used in order to assess the corrosion mechanisms and the involved phenomena and to correlate them with the surface and the overall microstructural modifications.

Keywords: Titanium alloys, Solid particle erosion, Roughness, Aqueous corrosion.

Introduction

Titanium alloys, especially the most commercially available Ti6Al4V alloy, are widely used in aerospace, chemical, and automotive industries. They also find applications in surgery as medical implants due to their exceptional properties such as high specific strength, high toughness, low density, high working temperature, excellent corrosion resistance and biological inertness [1,2]. Yet, they present relatively poor wear resistance owing to their poor tribological properties [3-7].

Ti6Al4V alloy is an alpha plus beta type titanium alloy in which, a phase is crystallized in hexagonal close-packed (HCP) lattice and b phase crystallizes in body-centered cubic (BCC) lattice respectively. It is the most widely used titanium alloy and it can be found as a machining configuration, molding or a powder metallurgy product [2]. Depending on the heat treatment procedure, various microstructures can be obtained in Ti6Al4V alloy, such as lamellar, bi-modal and equiaxed microstructures [2,8]. Ti6Al4V alloy used in aerospace applications (specifically turbine blades) exposed to sand / dust due to environmental conditions (especially dust / sand storms in deserts) are subjected to solid particle erosion. Thus, erosion resistance renders as an important consideration in designing many critical components made out of Ti6Al4V alloy. More specifically, its structure can be exploited in numerous facilities such as blades and disks of aircraft compressors and gas turbines, helicopter rotor blanding valves, piping and centrifugal pumps used in waste water systems and sea water systems.

Solid particle erosion, a typical wear mode, is a process of progressive removal of material from a target surface that occurs in different machine parts due to the repeated impact of solid particles [9-12]. The effects of solid particle erosion, such as surface roughness, wear of components, surface degradation and reduction in the functional life of structure, have been recognized for a long time and it is a serious problem in many engineering systems [13,14]. It is a quite complex phenomenon, since it involves several processes. The main process is the mechanical impact, caused by the impingement of solid particles on the target material, secondary processes, like thermal, chemical and physical reactions between the counterparts are taking place during erosion [15-21].

As it is mentioned above, a reason that Ti6Al4V alloy is widely used is because of its excellent corrosion resistance [22-25]. It is well known that this capacity of the alloy is effected by a surface oxide while a passive film is formed rapidly on titanium in water. The film is rapidly regenerated even if it is destroyed. The surface film consist of TiO_2 and it is amorphous or of low crystallinity**.** Nevertheless, concerning the property of corrosion resistance, different measurements occur in case of a worn sample of Ti6Al4V alloy examined.

To sum up, the objective of this study is to estimate the influence of the particle impingement angle on the solid particle erosion behavior of Ti6Al4V alloy eroded with Al_2O_3 particles and then to observe its behavior on corrosion resistance in biological fluids, as well as to examine the possible way the solid particle erosion affect, by altering the Ti6Al4V surface characteristics, the subsequent electrochemical corrosion response.

Experimental Procedure

Ti6Al4V alloy used in this study was supplied by TIMET (Titanium & Medical & Mining Company, Turkey) in the form of 100 x 100 cm sheets (thickness of 1 mm). The samples were cut to sheets of 50 x 50 mm by using a cutting wheel (Accutom-5 by Struers). Specimens were cut from each sheet and prepared for metallographic examination. Traditional metallographic procedures were implemented, which included gridding by SiC papers (up to 1200grit) followed by polishing with diamond suspensions (1μm). Kroll's etch was used in order to reveal the microstructure of heat treated samples of Ti6Al4V. Inspection of all specimens was performed by Scanning Electron Microscopy (JEOL, GSM 6510CV SEM/ Oxford Instruments X-Act EDX). AX-ray diffraction (XRD) analysis has taken place in order to study the phase transformations and to identify the crystal structure of the Ti6Al4V sheet.

Solid particle erosion experiments, using a commercial sand-blasting chamber, were carried out at impact angles of 30°, 60° and 90° using angular Al_2O_3 particles (170 - 250 μm) as the erodent medium. Coupons were placed on the adjustable sample holder at the opposite side of the nozzle. The distance between the nozzle and the specimen was 10±1 mm, the pressure of the sprayed erodent from the nozzle, directly on the surface of the sample was 1 and 2 bars and the duration of each spraying was 10 min. Every 1 min, the material loss was recorded and the overall erosion rate was calculated from the mass loss versus the mass erodent of the experiment (triplicate runs). Erosion was quantified by mass loss measurement with an accuracy of 0.1 mg. The surface roughness of eroded Ti6Al4V specimens was examined by using an optical surface profilometer (TESA Rugosurf 10G).

Corrosion testing was conducted on coupons that were encapsulated in thermoset resin, leaving a surface area of ~$1cm^2$ to be exposed to Hanks' Balanced Salt solution at 25°C. All the electrochemical tests were performed using the Gill AC potentiostat/galvanostat by ACM Instruments. A standard three-electrode cell was employed, with Ag/AgCl (3.5 M KCl) as the reference electrode and a platinum gauge as the counter electrode. Potentiodynamic polarization tests were carried out at a scan rate of 10 mV/min, from -1000mV up to +1500mV. Polarization scanning started after 4 h of recording the Open Circuit Potential in Hanks' Balanced Salt solution at 25°C. Reverse polarization was conducted to study the susceptibility of the specimens to localized corrosion.

Results and Discussion

Ti - 6Al - 4V Characterization

The microstructure of the Ti6Al4V sheet (surface and cross section) is illustrated in Figure 1. Regarding to the microstructural characterization, Figure 1(a) and (b) shows the equiaxed microstructural feature of Ti - 6Al - 4V. Compared to the literature [26,27], we deduce that the alloy sheet consists of a granular primary a-phase (darker regions) and a b-phase plus acicular a-phase (brighter regions) along the grain boundaries. This microstructure of the alloy is a result of annealing at the a+b region (<995°C) with a very slow cool from 927°C to room temperature for 1hour. The X-ray diffraction pattern of the Ti6Al4V (Figure 1c) shows that the alloy obtains mostly ana-phase which crystallizes in HCP lattice and a b-phase crystallized in BCC lattice.

Solid particle erosion behavior – Eroded surfaces morphology

The erosion rates of the examined materials are displayed in Figure 2(a). It can be observed that at higher impingement angles the erosion behavior of Ti6Al4V is improved significantly. As stated by other researchers [28-35], ductile materials exhibit a maximum in the erosion rate at intermediate impact angles (30°). In contrast, the maximum erosion rate of a brittle material is usually obtained at higher impact angle (90°). As a result, this behavior most likely suggests an overall ductile mode of erosion and material removal mode. This ductile character is most likely associated with the presence of the BCCb-phase in the alloy and generally the initial microstructure of the examined material.

As for the different applied pressure of erodent particles

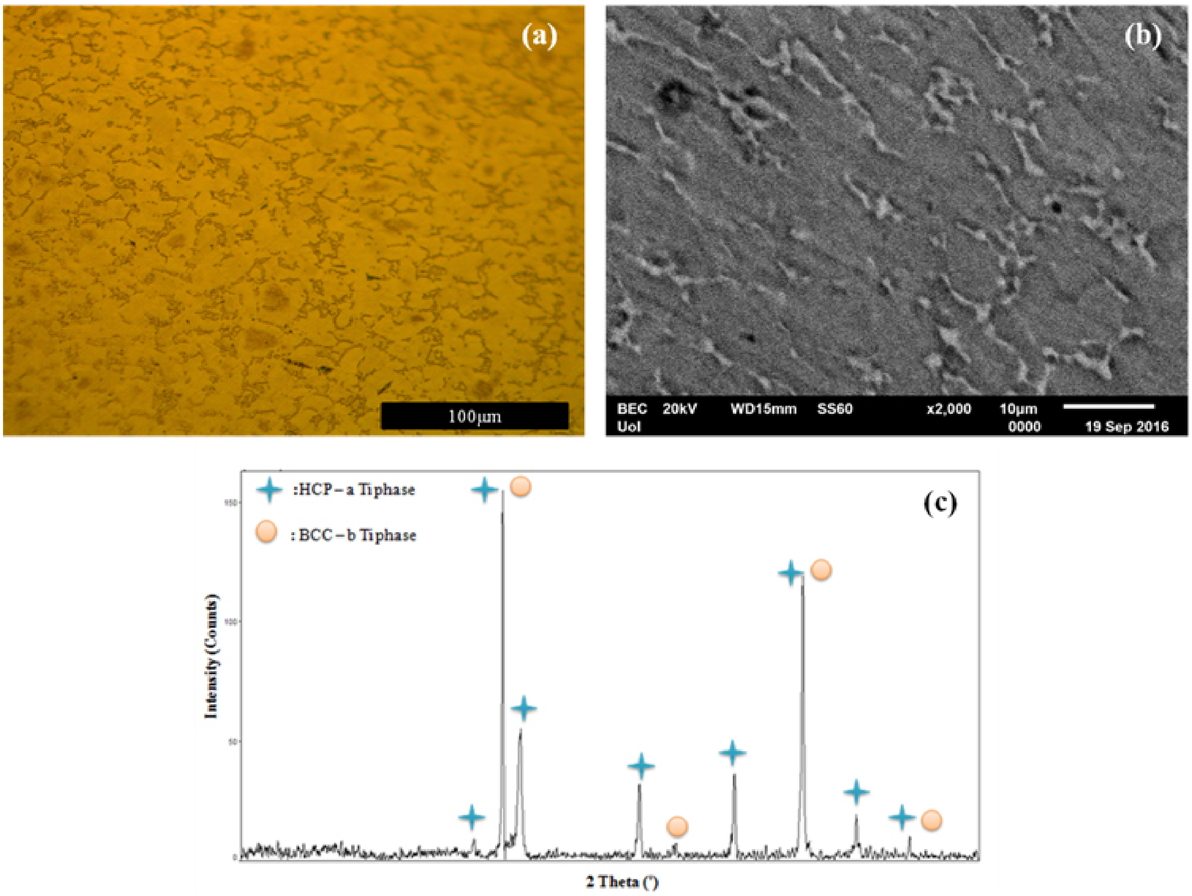

Figure 1: Microstructure (SEM-BEC mode) of the Ti6Al4V (a) surface and (b) cross section of the initial microstructure and (c) XRD analysis of the examined material

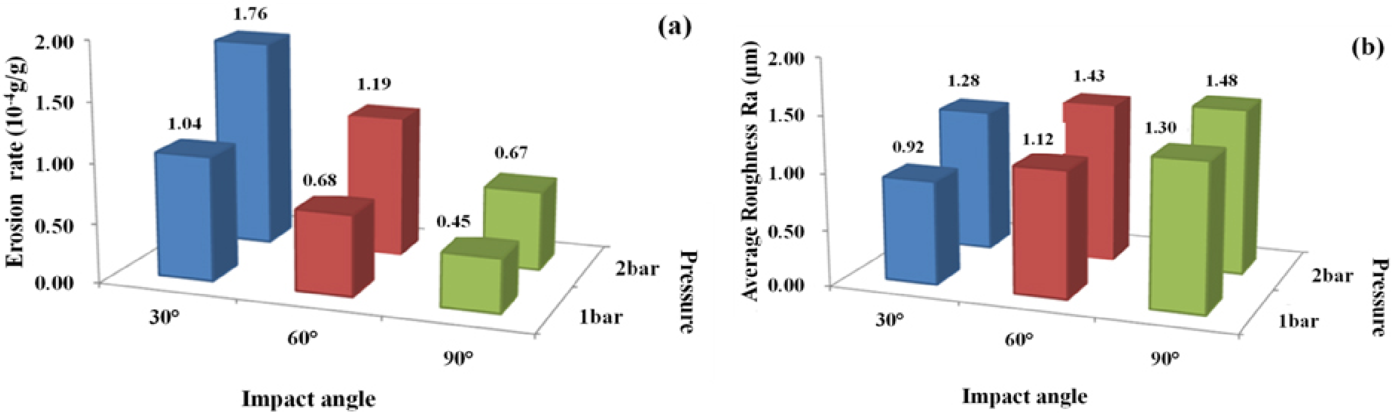

Figure 2: Erosion rates (a) and average surface roughness (b) of the eroded materials at different pressures and impact angles

it is generally established that the applied pressure alters the erodent particle velocity, in a proportional way. Other researchers have also extensively investigated the particle velocity effect on the solid particle erosion behavior of materials [32,36-48]. Figure 2(a) shows erosion rates of samples as a function of particle pressure at 30°, 60° and 90° impingement angles. It can be seen that erosion rates of samples increase with increasing particle pressure for all impingement angles. On the other hand, increase in the particle impingement pressure does not alter the erosion behavior of Ti6Al4V alloy, and samples exhibit ductile erosion behavior by showing maximum erosion at 30° impingement angle at various pressures.

Surface morphology (topography and roughness) plays, or could play an important role in surface analysis after erosion by particles. Alongside weight loss, more detailed information can be obtained by measuring surface roughness after erosion. Roughness (micro-roughness) parameter was measured before (Ra= 0.1734 ± 0.0492 μm) and after erosion with Al_2O_3 particles at 1 and 2 bar pressure and 30°, 60° and 90° angles of impingement, using a profilometer. The main roughness parameter which was obtained from this test was Ra – the roughness average. Value changes of the Ra parameter, in dependence of angle of impact and erodent pressure, are shown in Figure 2b.

Based on obtained weight loss results, selected and presented values of roughness parameters correlate with erosion rates. It can be seen that roughness significantly changes depending on the impingement angle. It is observed that surface roughness is increased with increasing the particle impingement angle. When the applied pressure is increasing the average surface roughness also increases. Similar results were found by other researchers [49].

As stated earlier, during the solid particle erosion process, dominant erosion mechanism strongly affects the solid particle erosion behavior of materials. Surface morphology of eroded surfaces may help to determine whether erosion has occurred via a ductile or brittle mechanism [50]. Therefore, eroded surfaces of Ti6Al4V samples were investigated by SEM in order to understand solid particle erosion behavior of samples under various parameters (particle impingement angle and applied pressure). Figure 3 shows the topology of the eroded surfaces for the different materials tested. Intensive landscape with extended and deep grooves can be observed in all cases, which is characteristic of severe plastic deformation. Ductile materials undergo wear by a process of plastic deformation in which the material is removed by the displacing or cutting action of the eroding particles [29,33,34]. These mechanisms are called micro-cutting and micro-ploughing, and dominantly erode ductile materials at acute impingement angles (15° and 30°).

The landscape, however, seems to become harsher as the impact angle and applied pressure increase. At normal impingement angle (90°), wear mechanism is dominated by plastic deformation and propagation of multiple cracks in all directions by repeated impacts of erodent particles. However, such damage cannot lead to effective removal of material due to ductile behavior of Ti6Al4V alloy. Therefore, at 90° impingement angle, limited wear tracks and plastic deformations are observed, which cause lower erosion rates compared to 30° impingement angle. Micro-cracks and plastic deformed regions were observed due to penetration of accelerated particles into the sample surfaces; this type of erosion mechanisms cannot effectively erode ductile materials. Hence, minimum erosion rate was observed at 90° impingement angle for Ti6Al4V alloy. Moreover, embedded particles were observed inside the eroded surfaces, as illustrated in Figure 3. At every examined impingement angle, erodent particles can embed to ductile materials such as Ti6Al4V alloy. Energy dispersive X-ray spectroscopy mapping indicates the presence of alumina particles (Al_2O_3) on the eroded surfaces of samples.

Corrosion performance of eroded Ti6Al4V alloy

Figure 4 demonstrates the potentiodynamic polarization behavior of the eroded Ti6Al4V specimens at different impingements angles at applied pressure 2 bar including that of neat Ti6Al4V.

In general the corrosion potential of the specimens which were eroded is lower than of the neat Ti6Al4V because the fact that the eroded specimens exhibit a layer of Al_2O_3 which protect them from corrosion in Hank's solution. All compositions present passivation over large ranges of anodic potentials; however, the high values of passive currents (>0.1 mA/cm^2) indicate pseudopassivity, as stated by other researchers [3,23-25].

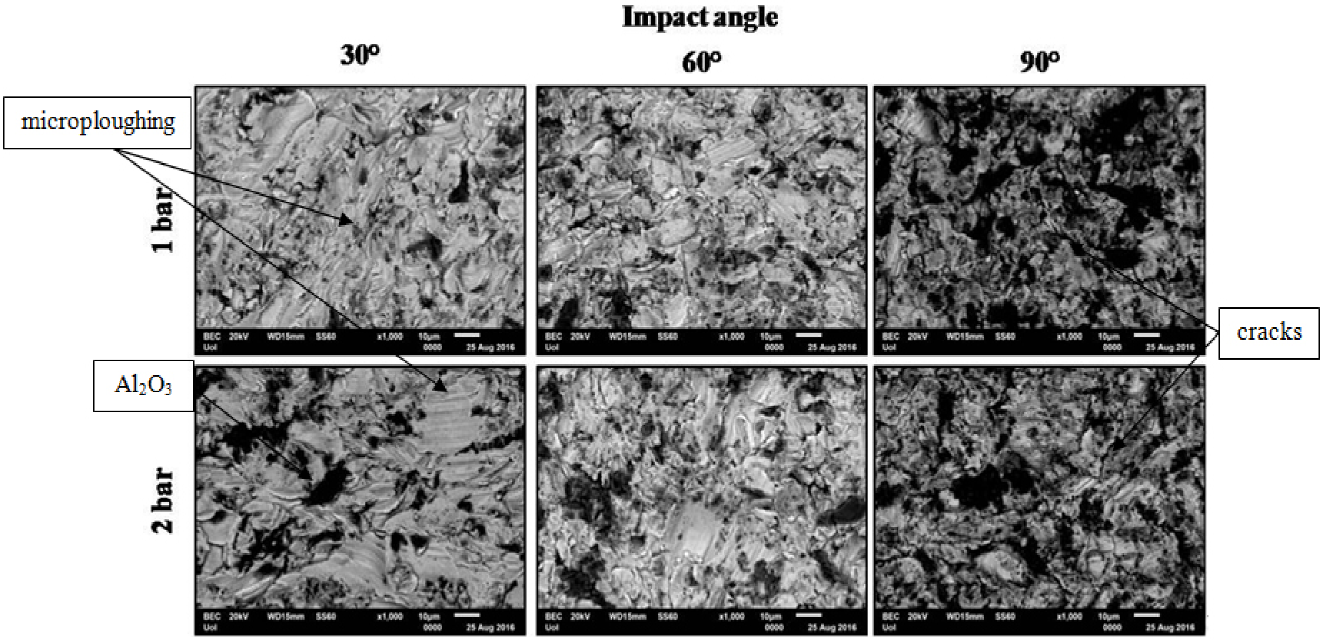

Figure 3: Topography of the eroded surfaces

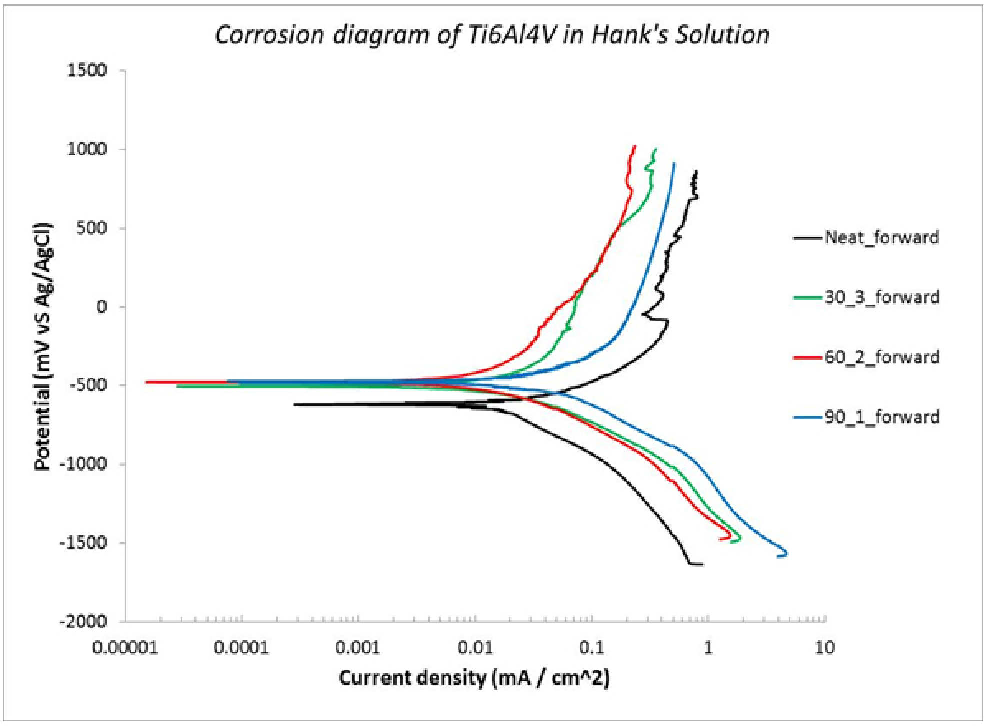

Figure 4: Forward polarization curves of the different specimens tested in present effort

Moreover, at the areas, which are not fully covered with Al_2O_3 due to the solid particle erosion experiments, valleys are developed in which localized corrosion phenomena are occurring. In more detail, corrosion pits are present due to the formation of galvanic cells in which the bottom of the valley acts as anode whereas the near the valley areas, which are mainly Al_2O_3, act as cathode.

As the corrosion potential values reaches the values of the passivitation area, corrosion products are formed above the described earlier pits. Due to the fact, at the bottom of the pits hydrolysis may occur, the corrosion products possibly are quite unstable (Figure 5) and as a result high currents are detected by the galvanostat due to the low conductivity of the formed corrosion products. Thick hydrated salts are continuing to form rapidly raising the current. As a result, the currents which are detected at the passivitation area (which is the sum of the average value of currents at areas which are covered with Al_2O_3 – low current areas – and the average value of currents at pits which are covered with corrosion products – high current areas-) exhibit high values leading at a pseudopassivity state.

At the neat Ti6Al4V, the main degradation morphology is intergranular corrosion occurring mainly atthe grain boundaries (Figure 6). The microstructural observations correlate well with the potentiodynamic polarization performance of the eroded materials, with respect to the following aspect: erodent Al_2O_3 particles were embedded to the grain boundaries of the a–phase and as a result protect the erodent Ti6Al4V from intergranular corrosion.

Concerning the specimens which were subjected to solid particle erosion at impingement angle 30°, pitting corrosion is not quite extensive since the anodic-to-cathodic transition potential ($E_{a/c\ tr}$) exhibit similar values and the hysteresis loop is quite small. The exact same observations are occurring and to the specimens which were subjected to solid particle erosion at impingement angle 60°. As for the specimens which were subjected to solid particle erosion at impingement angle 90°, the hysteresis loops are slightly positive which at the active state becomes negative. This means that, while the eroded specimens is corroded at the active state, corrosion pitting is also observed which also is explained by the higher average micro-roughness of the eroded surface. In this case also the presence of embedded Al_2O_3 lead protection during the pseudopassivity state. In general the examined materials exhibit adequate corrosion behavior towards Hank's solution.

Conclusions

1. Particle impingement angle dramatically affects solid particle erosion behavior of Ti6Al4V alloy. Ti6Al4V alloy shows ductile erosion behavior, and maximum erosion rate occurs at 30° impingement angle.
2. Erosion rate of Ti6Al4V alloy increases by increase in particle velocities.
3. Scanning electron microscopy investigations of eroded surfaces of Ti6Al4V alloy samples reveal the dominance erosion mechanism such as micro-ploughing, micro-cutting and plastic deformation at various parameters. Dominance erosion mechanism varied depending on the particle impingement angle. Particle impingement velocity and erodent particle size

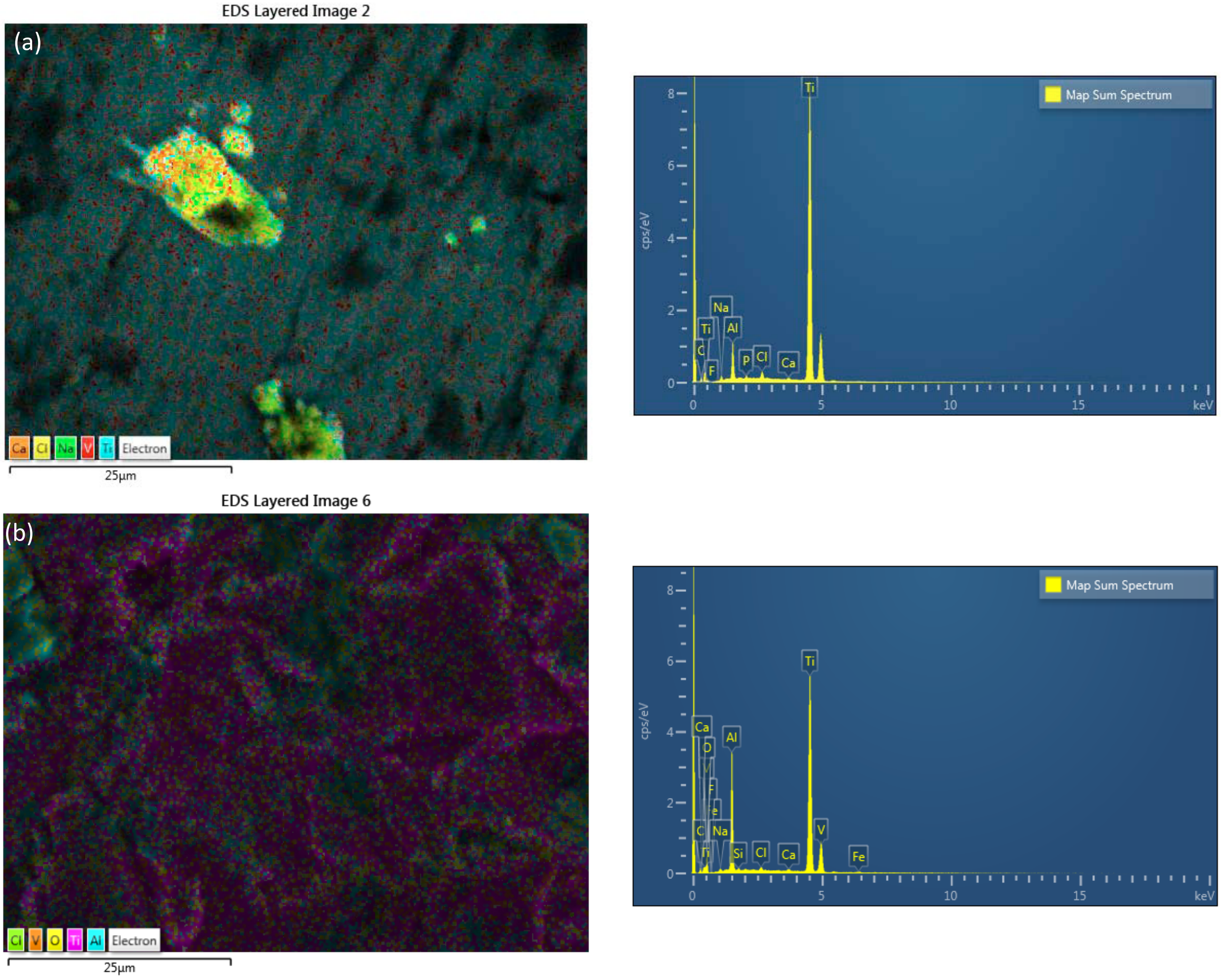

Figure 5: (a) EDX spectrum of neat Ti6Al4V surface after electrochemical corrosion in Hank's solution and (b) EDX spectrum (60° impingement angle) which indicates that inside the corrosion pits water soluble corrosion products are formed

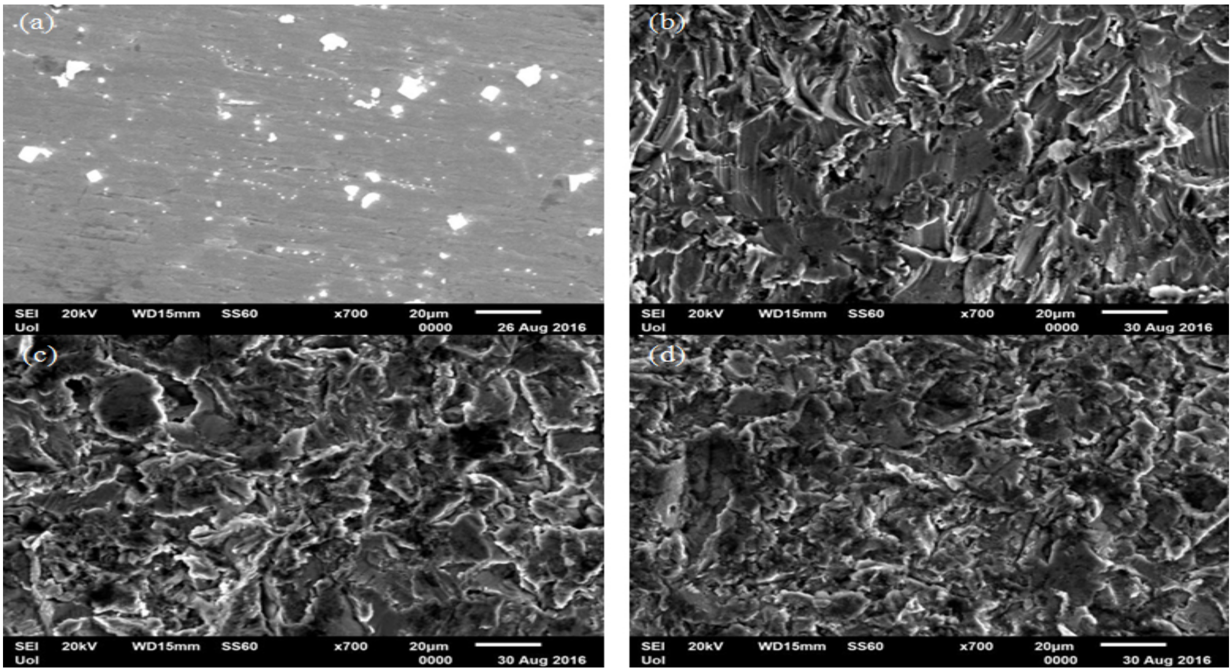

Figure 6: Plane view (secondary electron mode) of (a) neat Ti6Al4V (Presence of extensive bright spots network at the grain boundaries for the neat material. This presence most likely indicates an intergranular mode of the corrosive degradation phenomena.), (b) eroded Ti6Al4V (30° impingement angle), (c) eroded Ti6Al4V (60° impingement angle) and (d) eroded Ti6Al4V (90° impingement angle) after electrochemical corrosion in Hank's solution

do not affect dominant erosion mechanism. These parameters affect the scale of damage caused by solid particle erosion. Scanning electron microscopy results are also well correlated with erosion rates.

4. The surfaces roughness of the samples was dramatically affected by both particle impingement angle and velocity. Surface roughness values obtained by profilometer showed that average roughness of the samples was increased with augmentation in particle impingement angle and velocity.
5. The polarization behavior in Hank's solution is characterized localized pitting corrosion phenomena.
6. The corrosion potential of the specimens which were eroded is lower than of the neat Ti6Al4V because the fact that the eroded specimens exhibit a layer of embedded Al_2O_3 which protect them from corrosion in Hank's solution.

Acknowledgements

Authors would like to thank Prof. Sofoklis Makridis who applied us part of the arc-melting apparatus system under his patent https://www.researchgate.net/publication/200664162_Multiapparatus_Arc_Melting_for_Rapid_Solidification_Processes?ev=prf_pub.

References

1. Rack HJ, Qazi JI. Titanium alloys for biomedical applications. Materials Science and Engineering: C. 2006; 26(8):1269-1277. doi: http://dx.doi.org/10.1016/j.msec.2005.08.032.
2. Bomberger HB, Froes FH, Morton PH. Titanium-A Historical Perspective. In: Froes FH, Eylon D, Bomberger HB. Titanium Technology: Present Status and Future Trends. Titanium Developement Association; 1985. p. 3-17.
3. Manhabosco TM, Tamborim SM, dos Santos CB, Müller IL. Tribological, electrochemical and tribo-electrochemical characterization of bare and nitrided Ti6Al4V in simulated body fluid solution. Corrosion Science. 2011; 53(5):1786-1793. doi: http://dx.doi.org/10.1016/j.corsci.2011.01.057.
4. Li J, Sun M, Ma X, Tang G. Structure and tribological performance of modified layer on Ti6Al4V alloy by plasma-based ion implantation with oxygen. Wear. 2006; 261(11-12):1247-1252. doi: http://dx.doi.org/10.1016/j.wear.2006.03.010.
5. Martini C, Ceschini L. A comparative study of the tribologicalbehaviour of PVD coatings on the Ti-6Al-4V alloy. Tribology International. 2011; 44(3):297-308. doi: http://dx.doi.org/10.1016/j.triboint.2010.10.031.
6. Yetim AF, Celik A, Alsaran A. Improving tribological properties of Ti6Al4V alloy with duplex surface treatment. Surface and Coatings Technology. 2010; 205(2):320-324. doi: http://dx.doi.org/10.1016/j.surfcoat.2010.06.048.
7. Yetim AF, Yildiz F, Vangolu Y, Alsaran A, Celik A. Several plasma diffusion processes for improving wear properties of Ti6Al4V alloy. Wear. 2009; 267(12):2179-2185. doi: http://dx.doi.org/10.1016/j.wear.2009.04.005.
8. Chraponski J, Szkliniarz W. Quantitative metallography of two-phase titanium alloys. Materials characterization. 2001; 46(2-3):149-154. doi: http://dx.doi.org/10.1016/S1044-5803(01)00117-6.
9. Barkoula NM, Karger Kocsis J. Review: Processes and influencing parameters of the solid particle erosion of polymers and their composites. Journal of Materials Science. 2002; 37(18):3807-3820. doi: http://dx.doi.org/10.1023/A:1019633515481.
10. Avcu E, Fidan S, Bora MÖ, Çoban O, Taskiran I, Sinmazçelik T. Solid Particle Erosive Wear Behavior of Glass Mat Reinforced PPS Composites: Influence of Erodent Particle Size, Pressure, Particle Impingement Angle, and Velocity. Advances in Polymer Technology. 2013; 32(51):386-398. doi: http://dx.doi.org/10.1002/adv.21286.
11. Sinmazçelik T, Fidan S, Günay V. Residual mechanical properties of carbon/polyphenylenesulphide composites after solid particle erosion. Materials & Design. 2008; 29(7):1419-1426. doi: http://dx.doi.org/10.1016/j.matdes.2007.09.003.
12. Gousia V, Tsioukis A. Lekatou A, Karantzalis AE. Al-$MoSi_2$Composite Materials: Analysis of Microstructure, Sliding Wear, Solid Particle Erosion, and Aqueous Corrosion. Journal of Materials Engineering and Performance. 2016; 25(8):3107-3120. doi: http://dx.doi.org/10.1007/s11665-016-1947-1.
13. Yerramareddy S, Bahadur S. Effect of operational variables, microstructure and mechanical properties on the erosion of Ti-6Al-4V. Wear. 1991; 142(2):253-263. doi: http://dx.doi.org/10.1016/0043-1648(91)90168-T.
14. Zhou J, Bahadur S. Erosion-corrosion of Ti-6Al-4V in elevated temperature air environment. Wear. 1995; 186-187(1):332-339. doi: http://dx.doi.org/10.1016/0043-1648(95)07161-X.
15. Finnie I. The Mechanisms of Erosive Wear in Ductile Metal. In: Corrosion-Erosion Behavior of Materials: Proceedings of a symposium. Natesan K, editor. New York: AIME; 1980. p. 118-126.
16. Hutchings IM. Mechanisms of the Erosion of Metals by Solid Particles. In: STP664 - Erosion: Prevention and Useful Applications. ASTM. 1977. doi: http://dx.doi.org/10.1520/STP35795S.
17. Finnie I, Levy A, McFadden DJ. Fundamental Mechanisms of the Erosive Wear of Ductile Metals by Solid Particles. In: STP664 - Erosion: Prevention and Useful Applications. ASTM. 1979; 36–38. doi: http://dx.doi.org/10.1520/STP35795S.
18. Tu JP, Pan J, Matsumura M, Fukunaga H. The solid particle erosion behavior of $Al_{18}B_4O_{33}$ whisker-reinforced AC4C al alloy matrix composites. Wear. 1998; 223(1-2):22–30. doi: http://dx.doi.org/10.1016/S0043-1648(98)00295-6.
19. Fang Q, Sidky P, Hocking MG. Erosive wear behaviour of aluminium based composites. Materials & Design. 1998; 18(4-6):389–393. doi: http://dx.doi.org/10.1016/S0261-3069(97)00081-2.
20. Acharya SK, Dikshit V, Mishra P. Erosive Wear Behaviour of Redmud Filled Metal Matrix Composite. Journal of Reinforced Plastics and Composites. 2008; 27(2):145–152. doi: https://doi.org/10.1177/0731684407082543.
21. Wilson S, Ball A. Wear Resistance of an Aluminium Matrix Composite. In: Rohatgi PK, Blau PJ, Yust CS, editors. Tribology of Composite Materials: proceedings of a conference. Metals Park, OH: ASM International; 1990. p. 103–112.

22. Velten D, Biehl V, Aubertin F, Valeske B, Possart W, Breme J. Preparation of TiO_2 layers on cp-Ti and Ti6Al4V by thermal and anodic oxidation and by sol-gel coating techniques and their characterization. Journal of Biomedical Materials Research. 2001; 59(1):18-28. doi: http://dx.doi.org/10.1002/jbm.1212.
23. Cigada A, Cabrini M, Pedeferri P. Increasing of the corrosion resistance of the Ti6Al4V alloy by high thickness anodic oxidation. Journal of Materials Science: Materials in Medicine. 1991; 3(6):408-412. doi: http://dx.doi.org/10.1007/BF00701236.
24. Khan MA, Williams RL, Williams DF. In-vitrocorrosion and wear of titanium alloys in the biological environment. Biomaterials. 1996; 17(22):2117-2126. doi: http://dx.doi.org/10.1016/0142-9612(96)00029-4.
25. Karpagavalli R, Zhou A, Chellamuthu P, Nguyen K. Corrosion behavior and biocompatibility of nanostructured TiO_2 film on Ti6Al4V. Journal of Biomedical Materials Research - Part A. 2007; 83(4):1087-1095. doi: http://dx.doi.org/10.1002/jbm.a.31447.
26. Available from: http://www.timet.com/products/sheet.
27. Gammon LM, Briggs RD, Packard JM, Batson KW, Boyer R, Domby CW. Metallography and microstructures of Titanium and its alloys in Metallography and Microstructurs. ASM Handbook, ASM International; 2004. p. 899-917.
28. Jha AK, Batham R, Ahmed M, Majumder AK, Modi OP, Chaturvedi S, et al. Effect of impinging angle and rotating speed on erosion behavior of aluminum. Transactions of Nonferrous Metals Society of China. 2011; 21(1):32-38. doi: http://dx.doi.org/10.1016/S1003-6326(11)60674-2.
29. Finnie I. Some Reflections on the Past and Future of Erosion. Wear. 1995; 186-187(1):1-10. doi: http://dx.doi.org/10.1016/0043-1648(95)07188-1.
30. Hung FY, Chen LH, Lui TS. Impact angle of maximum erosion rate of wear resistant spheroidal graphite cast iron eroded by SiO2 and Al2O3 particles. International Journal of Cast Metals Research. 2003; 16(5):505-513. doi: http://dx.doi.org/10.1179/136404603225007872.
31. Lopez D, Congote JP, Cano JR, Toro A, Tschiptschin AP. Effect of particle velocity and impact angle on the corrosion–erosion of AISI 304 and AISI 420 stainless steels. Wear. 2005; 259(1-6):118-124. doi: http://dx.doi.org/10.1016/j.wear.2005.02.032.
32. Oka YI, Mihara S, Yoshida T. Impact-angle dependence and estimation of erosion damage to ceramic materials caused by solid particle impact. Wear. 2009; 267(1-4):129-135. doi: http://dx.doi.org/10.1016/j.wear.2008.12.091.
33. Oka YI, Ohnogi H, Hosokawa T, Matsumura M. The impact angle dependence of erosion damage caused by solid particle impact. Wear. 1997; 203-204:573-579. doi: http://dx.doi.org/10.1016/S0043-1648(96)07430-3.
34. Sundararajan G, Roy M. Solid particle erosion behaviour of metallic materials at room and elevated temperatures. Tribology International. 1997; 30(5):339-359. doi: http://dx.doi.org/10.1016/S0301-679X(96)00064-3.
35. Wood RJK. Erosion–corrosion interactions and their effect on marine and offshore materials. Wear. 2006; 261(9):1012-1023. doi: http://dx.doi.org/10.1016/j.wear.2006.03.033.
36. Biswas S, Satapathy A. Tribo-performance analysis of red mud filled glass-epoxy composites using Taguchi experimental design. Materials & Design. 2009; 30(8):2841-2853. doi: http://dx.doi.org/10.1016/j.matdes.2009.01.018.
37. Burzynski T, Papini M. Analytical model of particle interference effects in divergent erosive jets. Tribology International. 2010; 43(3):554-567. doi: http://dx.doi.org/10.1016/j.triboint.2009.09.004.
38. Chen Q, Li DY. Computer simulation of solid particle erosion. Wear. 2003; 254(3-4):203-210. doi: http://dx.doi.org/10.1016/S0043-1648(03)00006-1.
39. Deng T, Bingley MS, Bradley MSA. Understanding particle dynamics in erosion testers - A review of influences of particle movement on erosion test conditions. Wear. 2009; 267(11):2132-2140. doi: http://dx.doi.org/10.1016/j.wear.2009.02.020.
40. Gandhi BK, Borse SV. Nominal particle size of multi-sized particulate slurries for evaluation of erosion wear and effect of fine particles. Wear. 2004; 257(1-2):73-79. doi: http://dx.doi.org/10.1016/j.wear.2003.10.013.
41. Harsha AP, Jha SK. Erosive wear studies of epoxy-based composites at normal incidence. Wear. 2008; 265(7-8):1129-1135. doi: http://dx.doi.org/10.1016/j.wear.2008.03.003.
42. Harsha AP, Tewari US, Venkatraman B. Solid particle erosion behaviour of various polyaryletherketone composites. Wear. 2003; 254(7-8):693-712. doi: http://dx.doi.org/10.1016/S0043-1648(03)00143-1.
43. Harsha AP, Thakre AA. Investigation on solid particle erosion behaviour of polyetherimide and its composites. Wear. 2007; 262(7-8):807-818. doi: http://dx.doi.org/10.1016/j.wear.2006.08.012.
44. Patnaik A, Satapathy A, Chand N, Barkoula NM, Biswas S. Solid particle erosion wear characteristics of fiber and particulate filled polymer composites: A review. Wear. 2010; 268(1-2):249-263. doi: http://dx.doi.org/10.1016/j.wear.2009.07.021.
45. Sinmazcelik T, Fidan S, Gunay V. Residual mechanical properties of carbon/polyphenylenesulphide composites after solid particle erosion. Materials & Design. 2008; 29(7):1419-1426. doi: http://dx.doi.org/10.1016/j.matdes.2007.09.003.
46. Sinmazcelik T, Sari NY. Erodent size effect on the erosion of polyphenylene sulfide composite. Polymer Composites. 2010; 31(6):985-994. doi: http://dx.doi.org/10.1002/pc.20883.
47. Sinmazcelik T, Taskiran I. Erosive wear behaviour of polyphenylenesulphide (PPS) composites. Materials & Design. 2007; 28(9):2471-2477. doi: http://dx.doi.org/10.1016/j.matdes.2006.08.007.
48. Srivastava VK. Effects of wheat starch on erosive wear of E-glass fibre reinforced epoxy resin composite materials. Materials Science and Engineering: A. 2006; 435-436:282-287. doi: http://dx.doi.org/10.1016/j.msea.2006.07.144.
49. Curkovic L, Kumic I, Grilec K. Solid particle erosion behaviour of high purity alumina ceramics. Ceramics International. 2011; 37(1):29-35. doi: http://dx.doi.org/10.1016/j.ceramint.2010.08.029.
50. Suresh A, Harsha AP, Chosh MK. Solid particle erosion studies on polyphenylene sulfide composites and prediction on erosion data using artificial neural networks. Wear. 2009; 266(1-2):184-193. doi: http://dx.doi.org/10.1016/j.wear.2008.06.008.